

G^1 Hermite Interpolation by Minkowski Pythagorean Hodograph Cubics

Jiří Kosinka and Bert Jüttler *

*Johannes Kepler University, Institute of Applied Geometry, Altenberger Str. 69,
A-4040 Linz, Austria*

Abstract

As observed by Choi et al. (1999), curves in Minkowski space $\mathbb{R}^{2,1}$ are very well suited to describe the medial axis transform (MAT) of a planar domain, and Minkowski Pythagorean hodograph (MPH) curves correspond to domains, where both the boundaries and their offsets are rational curves (Moon, 1999). Based on these earlier results, we give a thorough discussion of G^1 Hermite interpolation by MPH cubics, focusing on solvability and approximation order. Among other results, it is shown that any analytic space-like curve without isolated inflections can be approximately converted into a G^1 spline curve composed of MPH cubics with the approximation order being equal to four. The theoretical results are illustrated by several examples. In addition, we show how the curvature of a curve in Minkowski space is related to the boundaries of the associated planar domain.

Key words: Hermite interpolation, Minkowski Pythagorean hodograph curves, space-like vector, Taylor expansion.

1 Introduction

Offsets of planar curves are needed for various applications. For example, they are used as the tool paths of computer-*numerical*-control (CNC) machines. Since the accuracy and efficiency of the representation of curves and surfaces is one of the basic issues in computer aided geometric design (CAGD), curves with polynomial or rational offsets have been thoroughly investigated. In particular, Pythagorean hodograph (PH) curves, which were introduced by

* Corresponding author.

Email addresses: `Jiri.Kosinka@jku.at` (Jiří Kosinka), `Bert.Juettler@jku.at` (Bert Jüttler).

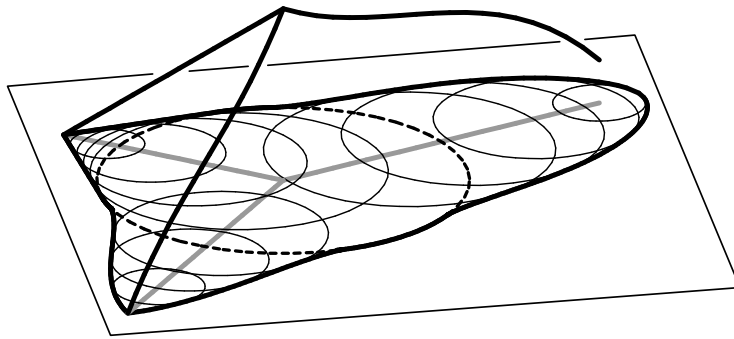


Fig. 1. The medial axis transform in xyr -space and the corresponding circles in the xy -plane. The envelope of the circles defines the boundary of the planar domain. The medial axis is shown in grey.

Farouki & Sakkalis (1990), are polynomial curves with rational offsets. Many related references can be found in the excellent survey of Farouki (2002).

In order to use the offset to a given curve as a tool path or for other applications, the so-called trimming procedure has to be applied. This procedure trims off the unwanted pieces and gives the true offset. Depending on the geometry and the offset distance, the trimming procedure can be time-consuming and computationally difficult.

An elegant approach to this problem was formulated by Moon (1999) and Choi et al. (1999). It is based on the medial axis transform (MAT) of a planar domain (see Pottmann and Peternell (1998) and Degen (2004), and the references cited therein) which identifies the domain with a (system of) space curve(s). Recall that the medial axis of a planar domain consists of the centers of all inscribed circles, which touch the boundary in at least two points. The MAT is then the system of space curves obtained by lifting the points of the medial axis of the domain into xyr -space, using the radius of the corresponding circle as additional coordinate, see Fig. 1.

Motivated by the offset formula for the boundaries of a planar domain, Moon defined MPH curves as polynomial speed curves in Minkowski (or pseudo-Euclidean) space with respect to Minkowski inner product. If the MAT is a (piecewise) MPH curve, the δ -offset curves to the corresponding boundary domain are rational. Moreover, the trimming procedure for the inner offsets becomes simpler, see Fig. 2 (cf. Pottmann and Peternell, 1998). The parts of the MAT, where the corresponding circle radius r is less than δ , have to be trimmed.

Based on so called domain decomposition technique, Choi et al. (1999) have designed an interpolation scheme for interpolating the MAT of a planar domain by MPH cubics. Recently, Kim & Ahn (2003) addressed the problem of C^1 Hermite interpolation using MPH quartics and introduced a new con-

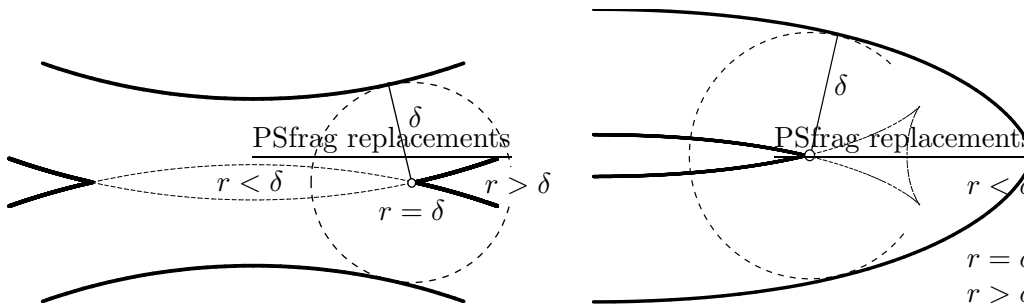


Fig. 2. Trimming procedure using medial axis transform.

cept, $C^{1/2}$ interpolation. MPH curves in higher dimensions have recently been analyzed by Cho et al. (2004).

The approximation of the MAT by pseudo-Euclidean arc splines and by parabolic arcs has been outlined by Pottmann and Peternell (1998).

Starting from the results of Choi et al. (1999), this paper analyzes the problem of G^1 Hermite interpolation by MPH cubics. Based on the mutual position of the given end tangent vectors, we formulate an algorithm for computing the interpolants in Bernstein-Bézier form. Lorentz transforms are used to map the given Hermite data to one among five canonical positions, which significantly simplify the analysis. The problem has in the ‘regular’ case four solutions, which can be computed by solving two quadratic equations.

Based on the canonical positions of the input data and the causal character of the difference of the end tangent vectors we derive sufficient and necessary conditions for interpolants to exist. In fact, the difference of the endpoints has to lie inside certain quadratic cones depending solely on the end tangent vectors. Singular cases are also discussed.

In order to analyze the convergence order of the interpolants, an asymptotic approach by means of Taylor expansions and Frenet formulas in Minkowski space is introduced. As a result, we give conditions for converting curves into MPH cubic splines. It turns out that any space-like (piecewise) analytic curve can be approximately converted into a G^1 MPH cubic spline. The approximation order is four, provided that the curve has no isolated inflections. Otherwise the approximation order drops to two.

In addition to these results on MPH cubics, we provide a geometric interpretation of the Minkowski curvature and Minkowski inflections in terms of the geometry of the associated planar domain.

2 Preliminaries

This section summarizes some basic concepts and some results concerning Minkowski space, MPH curves and differential geometry of curves in Minkowski space.

2.1 Minkowski space

The three-dimensional Minkowski space $\mathbb{R}^{2,1}$ is a real vector space with an indefinite inner product given by the matrix $G = \text{diag}(1, 1, -1)$. The inner product of two vectors $\mathbf{u} = (u_1, u_2, u_3)^\top$, $\mathbf{v} = (v_1, v_2, v_3)^\top$, $\mathbf{u}, \mathbf{v} \in \mathbb{R}^{2,1}$ is defined as

$$\langle \mathbf{u}, \mathbf{v} \rangle = \mathbf{u}^\top G \mathbf{v} = u_1 v_1 + u_2 v_2 - u_3 v_3. \quad (1)$$

The three axes spanned by the vectors $\mathbf{e}_1 = (1, 0, 0)^\top$, $\mathbf{e}_2 = (0, 1, 0)^\top$ and $\mathbf{e}_3 = (0, 0, 1)^\top$ will be denoted as the x -, y - and r -axis, respectively.

Since the quadratic form defined by G is not positive definite as in the Euclidean case, the square norm of \mathbf{u} defined by $\|\mathbf{u}\|^2 = \langle \mathbf{u}, \mathbf{u} \rangle$ may be positive, negative or zero. Motivated by the theory of relativity we distinguish three so-called ‘causal characters’ of vectors. A vector \mathbf{u} is called space-like if $\|\mathbf{u}\|^2 > 0$, time-like if $\|\mathbf{u}\|^2 < 0$, and light-like (or isotropic) if $\|\mathbf{u}\|^2 = 0$.

All light-like vectors form a cone in $\mathbb{R}^{2,1}$, the so called light cone. We denote a light cone with the vertex at a point \mathbf{w} by $\mathcal{C}_{\mathbf{w}}$.

Two vectors $\mathbf{u}, \mathbf{v} \in \mathbb{R}^{2,1}$ are said to be orthogonal if $\langle \mathbf{u}, \mathbf{v} \rangle = 0$. Therefore a normal vector of a plane given by $ax + by + cz = 0$ has the coordinates $\mathbf{n} = (a, b, -c)^\top$. The cross-product in the Minkowski space can be defined analogously to the Euclidean case as

$$\mathbf{w} = \mathbf{u} \times \mathbf{v} = (u_2 v_3 - u_3 v_2, u_3 v_1 - u_1 v_3, -u_1 v_2 + u_2 v_1)^\top. \quad (2)$$

Clearly, $\langle \mathbf{u}, \mathbf{u} \times \mathbf{v} \rangle = 0$ for all $\mathbf{u}, \mathbf{v} \in \mathbb{R}^{2,1}$.

A vector $\mathbf{u} \in \mathbb{R}^{2,1}$ is called a unit vector if $\|\mathbf{u}\|^2 = \pm 1$. When \mathbf{u} is a space-like vector, it can be normalized to $\|\mathbf{u}\|^2 = 1$, in the time-like case to $\|\mathbf{u}\|^2 = -1$.

2.2 Lorentz transforms

A linear transform $L : \mathbb{R}^{2,1} \rightarrow \mathbb{R}^{2,1}$ is called a Lorentz transform if it maintains the Minkowski inner product, i.e. $\langle \mathbf{u}, \mathbf{v} \rangle = \langle L\mathbf{u}, L\mathbf{v} \rangle$ for all $\mathbf{u}, \mathbf{v} \in \mathbb{R}^{2,1}$. The group of all Lorentz transforms $\mathcal{L} = O(2, 1)$ is called the Lorentz group.

Let $K = (k_{i,j})_{i,j=1,2,3}$ be a Lorentz transform. Then the column vectors \mathbf{k}_1 , \mathbf{k}_2 and \mathbf{k}_3 satisfy $\langle \mathbf{k}_i, \mathbf{k}_j \rangle = G_{i,j}$, $i, j \in \{1, 2, 3\}$, i.e., they form an orthonormal basis of $\mathbb{R}^{2,1}$.

From $\langle \mathbf{k}_3, \mathbf{k}_3 \rangle = G_{3,3} = -1$ one obtains $k_{33}^2 \geq 1$. A transform K is said to be *orthochronous* if $k_{33} \geq 1$. The determinant of any Lorentz transform K equals to ± 1 , and special ones are characterized by $\det(K) = 1$.

The Lorentz group \mathcal{L} consists of four components. The special orthochronous Lorentz transforms form a subgroup $SO_+(2, 1)$ of \mathcal{L} . The other components are $T_1 \cdot SO_+(2, 1)$, $T_2 \cdot SO_+(2, 1)$ and $T_1 \cdot T_2 \cdot SO_+(2, 1)$, where $T_1 = \text{diag}(1, 1, -1)$ and $T_2 = \text{diag}(1, -1, 1)$. Let

$$R(\alpha) = \begin{pmatrix} \cos \alpha & -\sin \alpha & 0 \\ \sin \alpha & \cos \alpha & 0 \\ 0 & 0 & 1 \end{pmatrix} \quad \text{and} \quad H(\beta) = \begin{pmatrix} 1 & 0 & 0 \\ 0 & \cosh \beta & \sinh \beta \\ 0 & \sinh \beta & \cosh \beta \end{pmatrix} \quad (3)$$

be a rotation of the spatial coordinates x , y , and a hyperbolic rotation with a hyperbolic angle β , respectively. Any special orthochronous Lorentz transform $L \in SO_+(2, 1)$ can be represented as $L = R(\alpha_1)H(\beta)R(\alpha_2)$.

2.3 Minkowski Pythagorean hodograph curves and the MAT

Recall that a polynomial curve in Euclidean space is said to be a Pythagorean hodograph (PH) curve, if the norm of its first derivative (or hodograph) is a (possibly piecewise) polynomial. Following Moon (1999), MPH curves are defined similarly, but with respect to the norm induced by the Minkowski inner product. More precisely, a polynomial curve $\mathbf{c} \in \mathbb{R}^{2,1}$, $\mathbf{c} = (x, y, z)^\top$ is called an MPH curve if a polynomial w exists such that

$$x'^2 + y'^2 - z'^2 = w^2. \quad (4)$$

We recall the motivation that led Moon (1999) to the definition of MPH curves. Consider a domain $\Omega \in \mathbb{R}^2$. The medial axis (MA) of Ω is the locus of all the centers of maximal disks touching the boundary $\partial\Omega$ in at least two points, which are inscribed into the domain Ω . Let $(x(t), y(t))^\top$ be a parameterization of a part of the medial axis of Ω and let $r(t)$ be a radius function, which specifies the radii of the maximal disks with centers at $(x(t), y(t))$. The corresponding part of the medial axis transform (MAT) is then a spatial curve $(x(t), y(t), r(t))^\top$.

On the other hand, given a segment $\mathbf{g}(t) = (x(t), y(t), r(t))^\top$, $t \in I$, of the MAT, we can recover the original domain by forming the union of the disks,

$$\Omega = \bigcup_{t \in I} D_{r(t)}(x(t), y(t)), \quad (5)$$

where $D_r(x, y)$ is the disk with center (x, y) and radius r . Its boundary $\partial\Omega$ is obtained as the envelope of the medial axis circles. The envelopes determined by a C^1 segment $\mathbf{g}(t) = (x(t), y(t), r(t))^\top$ of the MAT (see Choi et al., 1997) are

$$\mathbf{b}^{(\pm)}(t) = \begin{pmatrix} x \\ y \end{pmatrix} - \frac{r}{x'^2 + y'^2} \left[r' \begin{pmatrix} x' \\ y' \end{pmatrix} \pm \sqrt{x'^2 + y'^2 - r'^2} \begin{pmatrix} -y' \\ x' \end{pmatrix} \right], \quad (6)$$

provided that $r > 0$. Moreover, δ -offsets of $\partial\Omega$ may be computed the same way by lifting the MAT to $(x(t), y(t), r(t) \pm \delta)^\top$. As observed by Moon (1999), if the corresponding MAT is an MPH curve, then the coordinate functions of the envelopes are rational.

Remark 1 As an immediate consequence of the definition, the tangent vector $\mathbf{c}'(t)$ of an MPH curve cannot be time-like. Also, light-like tangent vectors $\mathbf{c}'(t)$ correspond to roots of the polynomial w in (4). In the remainder of this paper we consider only curves with space-like tangent vectors. These curves will be called space-like. Note that the MAT of a planar domain is a (collection of) space curve(s) with space-like or light-like tangent vectors, where the latter ones appear only at isolated points, typically at vertices (points with extremal curvature) of the boundaries.

2.4 Frenet formulas in Minkowski space

This section introduces several facts from the differential geometry of curves in the Minkowski space, cf. Blaschke (1929); Ekmekci & Ilarslan (1998); Walrave (1995). Consider a space-like curve $\mathbf{c}(s) \in \mathbb{R}^{2,1}$. We may assume that the curve is parameterized by its arc length, i.e. $\|\mathbf{c}'(s)\| = 1$. Then we define a (space-like) unit tangent vector $\mathbf{T} = \mathbf{c}'(s)$ of $\mathbf{c}(s)$. The Frenet formulas take the form

$$\begin{aligned} \mathbf{T}' &= \kappa \mathbf{N}, \\ \mathbf{N}' &= -\langle \mathbf{N}, \mathbf{N} \rangle \kappa \mathbf{T} + \tau \mathbf{B}, \\ \mathbf{B}' &= \tau \mathbf{N}, \end{aligned} \quad (7)$$

provided that the vector \mathbf{T}' of $\mathbf{c}(s)$ is space-like or time-like on some parameter interval. Then, the unit vectors \mathbf{N} and \mathbf{B} are the unit normal and binormal vector, respectively, and $\kappa > 0$ and τ are the Minkowski curvature and torsion of $\mathbf{c}(s)$. The three vectors \mathbf{T} , \mathbf{N} and \mathbf{B} form an orthonormal basis.

The vector \mathbf{T}' may be light-like at an isolated point, or within an entire interval. The two cases will be called (Minkowski) *inflections* and *inflected segments*, respectively. The first case will be addressed in the first paragraph of Section 5.2. In the second case, the Frenet formulas take the form

$$\begin{aligned} \mathbf{T}' &= \kappa \mathbf{N}, \\ \mathbf{N}' &= \tau \mathbf{N}, \\ \mathbf{B}' &= -\kappa \mathbf{T} - \tau \mathbf{B}, \end{aligned} \quad (8)$$

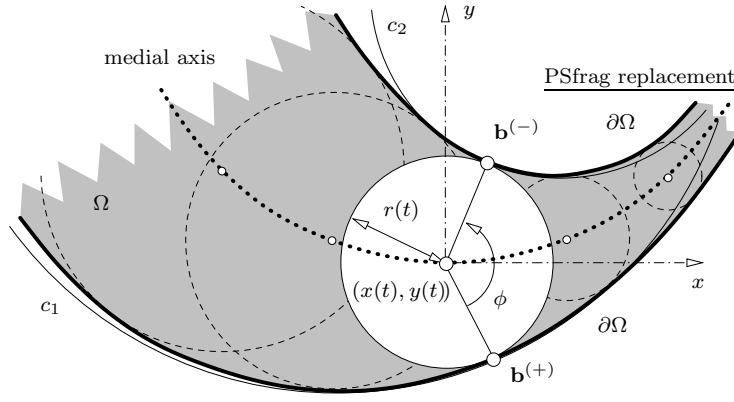


Fig. 3. A planar domain, its medial axis (dotted), an inscribed circle, and the curvatures of the boundaries (visualized by the osculating circles c_1 and c_2).

where $\langle \mathbf{T}, \mathbf{N} \rangle = \langle \mathbf{T}, \mathbf{B} \rangle = 0$, $\langle \mathbf{N}, \mathbf{N} \rangle = \langle \mathbf{B}, \mathbf{B} \rangle = 0$ and $\langle \mathbf{N}, \mathbf{B} \rangle = 1$. In this situation, the Minkowski curvature evaluates to $\kappa = 0$ if $\mathbf{c}(s)$ is a straight line, and to $\kappa = 1$ otherwise.

2.5 An interpretation of the Minkowski curvature

We discuss the relationship between the Minkowski curvature of a space-like curve in $\mathbb{R}^{2,1}$ and the curvatures of the boundaries of the associated planar domain. The results lead to an interpretation of Minkowski inflections and of inflected segments.

Proposition 2 *Let $\mathbf{p} = (x(t), y(t), r(t))^\top$ be a space-like curve in $\mathbb{R}^{2,1}$. Then*

$$\langle \mathbf{T}', \mathbf{T}' \rangle = \frac{1}{(\rho_1 - r)(\rho_2 + r) \sin^2 \frac{\phi}{2}} = \frac{k_1 k_2}{(1 - r k_1)(1 + r k_2) \sin^2 \frac{\phi}{2}}, \quad (9)$$

where \mathbf{T}' denotes the derivative of the unit tangent vector of \mathbf{p} with respect to the Minkowski arc length, $k_1 = \frac{1}{\rho_1}$, $k_2 = \frac{1}{\rho_2}$ are the signed curvatures according to the parameterization (6) of the boundaries of the associated planar domain Ω (see (5)), and the angle ϕ equals $\phi = \angle(\mathbf{b}^{(+)}, (x, y), \mathbf{b}^{(-)})$, cf. Figure 3.

Proof: We choose the coordinates such that the origin is located at $x(0), y(0)$, while the derivative $x'(0), y'(0)$ is aligned with the x -axis, see Figure 3. Then $\mathbf{b}^{(\pm)} = r(c, \mp s)$, where $c = \cos \frac{\phi}{2}$, $s = \sin \frac{\phi}{2}$. We replace the two boundary curves by their osculating circles c_1, c_2 at $\mathbf{b}^{(\pm)}$ with the radii ρ_i . The two circles define two light cones in $\mathbb{R}^{2,1}$ with apexes at

$$\mathbf{a}_1 = ((r - \rho_1)c, -(r - \rho_1)s, \rho_1)^\top \text{ and } \mathbf{a}_2 = ((r + \rho_2)c, (r + \rho_2)s, -\rho_2)^\top.$$

Each of them has a second order contact with the developable surface of constant slope $\pi/4$ through the corresponding boundary along the generating

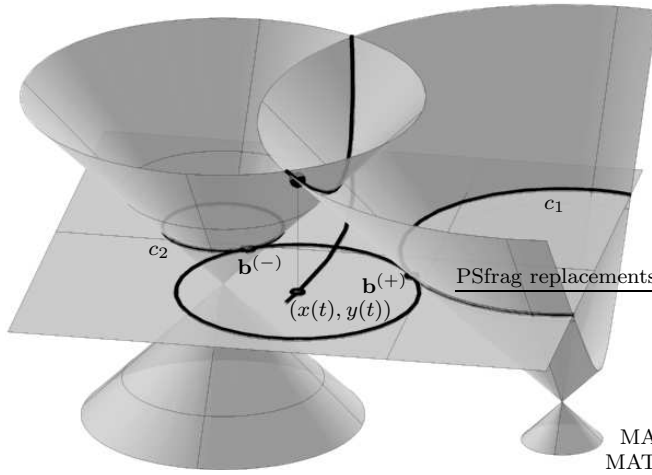


Fig. 4. Illustration of the proof of Proposition 2, via intersection of two circular cones. The conic and its projection into the xy plane is shown.

line through $\mathbf{b}^{(\pm)}$. The developable surfaces of constant slope are the graph surfaces of the signed distance functions associated with the boundaries.

One branch of the intersection curve of the light cones is a conic section (see Fig. 4), which has a contact of second order with the MAT $(x(t), y(t), r(t))^\top$ at the point $(0, 0, r(0))^\top$. It has the quadratic Taylor approximant

$$\mathbf{m}_2(\sigma) = \begin{pmatrix} 0 \\ 0 \\ r \end{pmatrix} + \frac{\sigma}{s} \begin{pmatrix} 1 \\ 0 \\ -c \end{pmatrix} + \frac{\sigma^2}{2} \mathbf{T}'(0) \quad (10)$$

with respect to the Minkowski arc length σ , where

$$\mathbf{T}'(0) = \frac{1}{2(\rho_1 - r)(\rho_2 + r)s^2} \begin{pmatrix} (2r - \rho_1 + \rho_2)c \\ (\rho_1 + \rho_2)s \\ -2r + \rho_1 - \rho_2 \end{pmatrix}. \quad (11)$$

Indeed, the quadratic Taylor approximant $\mathbf{m}_2(\sigma)$ satisfies approximately the equations of the light cones, $\|\mathbf{a}_i - \mathbf{m}_2(\sigma)\|^2 = \mathcal{O}(\sigma^3)$, and it also approximately satisfies the equations of the Minkowski arc length parameterization, $\|\mathbf{m}'_2(\sigma)\|^2 = 1 + \mathcal{O}(\sigma^2)$. Eq. (9) follows directly from (11). \square

Corollary 3 *If $\langle \mathbf{T}', \mathbf{T}' \rangle \neq 0$, then $\kappa = \sqrt{|\langle \mathbf{T}', \mathbf{T}' \rangle|}$. Consequently, Minkowski inflections correspond to inflections of at least one of the boundaries, and inflected segments correspond to planar domains where at least one of the boundaries is locally a straight line. Otherwise $\kappa = 0$ or $\kappa = 1$, see Section 2.4.*

3 Interpolation of G^1 Hermite boundary data

Consider an MPH cubic in Bézier form

$$\mathbf{g}(t) = \mathbf{p}_0 (1-t)^3 + \mathbf{p}_1 3t(1-t)^2 + \mathbf{p}_2 3t^2(1-t) + \mathbf{p}_3 t^3, \quad t \in [0, 1], \quad (12)$$

which is to interpolate the two given points $\mathbf{q}_0 = \mathbf{p}_0$ and $\mathbf{q}_1 = \mathbf{p}_3$, and the associated space-like unit tangent directions \mathbf{t}_0 and \mathbf{t}_1 . More precisely, we have to find constants a and b such that the inner control points satisfy

$$\mathbf{p}_1 = \mathbf{p}_0 + a\mathbf{t}_0, \quad \text{and} \quad \mathbf{p}_2 = \mathbf{p}_3 - b\mathbf{t}_1, \quad (13)$$

and the cubic is MPH. Since the degree of the hodograph $\mathbf{g}'(t)$ is two, this implies that there exists a quadratic polynomial

$$\sigma(t) = \sigma_0 (1-t)^2 + \sigma_1 2t(1-t) + \sigma_2 t^2 \quad (14)$$

such that $\|\mathbf{g}'(t)\|^2 = 9\sigma(t)^2$. Let

$$\mathbf{l}_0 = a\mathbf{t}_0, \quad \mathbf{l}_1 = (\mathbf{p}_3 - \mathbf{p}_0) - a\mathbf{t}_0 - b\mathbf{t}_1, \quad \mathbf{l}_2 = b\mathbf{t}_1, \quad (15)$$

be the legs of the control polygon of the cubic. The MPH condition leads to the five equations (cf. Choi et al., 1999)

$$\sigma_0^2 = \langle \mathbf{l}_0, \mathbf{l}_0 \rangle, \quad \sigma_2^2 = \langle \mathbf{l}_2, \mathbf{l}_2 \rangle, \quad (16)$$

$$\sigma_0\sigma_1 = \langle \mathbf{l}_0, \mathbf{l}_1 \rangle, \quad \sigma_1\sigma_2 = \langle \mathbf{l}_1, \mathbf{l}_2 \rangle \quad \text{and} \quad (17)$$

$$\sigma_0\sigma_2 + 2\sigma_1^2 = \langle \mathbf{l}_0, \mathbf{l}_2 \rangle + 2\langle \mathbf{l}_1, \mathbf{l}_1 \rangle. \quad (18)$$

The first two equations (16) are equivalent to $\sigma_0 = \pm a$ and $\sigma_2 = \pm b$. As $\sigma(t)$ and $-\sigma(t)$ yield the same hodograph $\mathbf{g}'(t)$, it suffices to consider only two of the four possible sign combinations,

$$\sigma_0 = a, \quad \sigma_2 = \pm b, \quad (19)$$

since the other two give the same results.

The first equation in (17) leads to

$$\sigma_1 = \langle \mathbf{t}_0, \mathbf{l}_1 \rangle. \quad (20)$$

After eliminating σ_1 from the two equations (17), and using (15) and (19), we arrive at one of the two equations

$$\langle \mathbf{l}_1, \mathbf{t}_0 \mp \mathbf{t}_1 \rangle = 0, \quad (21)$$

depending on the choice of the sign in $\sigma_2 = \pm b$.

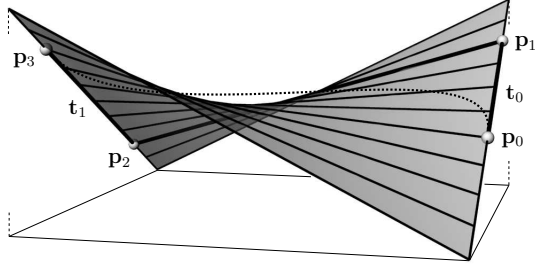


Fig. 5. Necessary condition: The control polygon of the interpolating MPH cubic lies on a certain hyperbolic paraboloid.

These equations form necessary conditions for the existence of a solution. From a geometric point of view, the leg \mathbf{l}_1 of the control polygon must be parallel to a plane with the normal vector $\mathbf{t}_0 \mp \mathbf{t}_1$ (with respect to Minkowski inner product). It is well known that all lines which are parallel to a given plane and intersect two skew lines form a hyperbolic paraboloid. Consequently, in the case of non-planar input data we get from each of the two cases in (21) such a hyperbolic paraboloid. The control polygons of the MPH cubics lie on these surfaces completely, see Fig. 5.

By substituting (19) and (20) into (18) we get one of the two equations

$$\pm ab + 2\langle \mathbf{t}_0, \mathbf{l}_1 \rangle^2 = ab\langle \mathbf{t}_0, \mathbf{t}_1 \rangle + 2\langle \mathbf{l}_1, \mathbf{l}_1 \rangle, \quad (22)$$

depending on the choice of sign in (19).

Finally we solve (21) for a and substitute the result into the corresponding equation (22). For each of the two cases, this leads to a quadratic equation $E_{1/2}(b) = 0$. Consequently, we may obtain up to four real solutions to the interpolation problem. The two equations $E_{1/2}(b) = 0$ are rather long, and we do not include them in a general expanded form. See Section 4 for canonical cases of these equations.

Let $E_i(b) = \phi_i b^2 + \xi_i b + \psi_i$, $\phi_1 \phi_2 \neq 0$, $\xi_i^2 - 4\phi_i \psi_i > 0$, where $i \in \{1, 2\}$. Then we denote the solutions as

$$b_{i,1} = \frac{-\xi_i + \sqrt{\xi_i^2 - 4\phi_i \psi_i}}{2\phi_i}, \quad b_{i,2} = \frac{-\xi_i - \sqrt{\xi_i^2 - 4\phi_i \psi_i}}{2\phi_i}. \quad (23)$$

The order of the solutions $b_{i,j}$ is important in the following discussions. Note that multiplying equations (22) by negative constants is not allowed, since it changes the labeling.

The algorithm for computing the interpolants is summarized in Table 1. An example will be presented later (see Section 6 and Fig. 12, page 23).

Table 1

 G^1 interpolation by MPH cubics.

| |
|---|
| <p>GIVEN: End points $\mathbf{q}_0, \mathbf{q}_1$ with associated space-like tangent vectors $\mathbf{t}_0, \mathbf{t}_1$.</p> <p>(1) Solve the equation $E_i(b)$ for b ($i = 1, 2$) $\implies b_{i,1}, b_{i,2}$.</p> <p>(2) Compute $a_{i,1}, a_{i,2}$ from $\langle \mathbf{I}_1, \mathbf{t}_0 \mp \mathbf{t}_1 \rangle = 0$ corresponding to $b_{i,1}, b_{i,2}$.</p> <p>OUTPUT: Four MPH cubic interpolants given by (12) and (13).</p> |
|---|

Remark 4 The two solutions obtained by choosing the plus signs in (19) corresponding to the plus sign in (22) and the minus sign in (21), which are found by solving $E_1(b) = 0$, will be called the *solutions of the first kind*. The other two solutions will be called the *solutions of the second kind*.

4 Solvability

This section studies the number of solutions for given G^1 input data. In order to analyze the solvability, we simplify the given input data without loss of generality as far as possible. First, we move the starting point $\mathbf{g}(0)$ of the curve $\mathbf{g}(t)$ to the origin, while the endpoint $\mathbf{g}(1)$ remains arbitrary, i.e.,

$$\mathbf{p}_0 = (0, 0, 0)^\top, \quad \mathbf{p}_3 = (x, y, r)^\top. \quad (24)$$

Then we apply Lorentz transforms in order to obtain one among five canonical positions, as described in the following section.

4.1 Canonical positions of the boundary tangents

Proposition 5 *Any pair of space-like unit vectors $\mathbf{t}_0, \mathbf{t}_1$ in three dimensional Minkowski space can be mapped by a Lorentz transform to one of the canonical positions described in Table 2, depending on the causal characters of their sum and difference vectors $\mathbf{s} = \mathbf{t}_0 + \mathbf{t}_1$ and $\mathbf{d} = \mathbf{t}_1 - \mathbf{t}_0$.*

Proof: The plane spanned by \mathbf{t}_0 and \mathbf{t}_1 can be space-like (case 1), time-like (cases 2 and 2') or light-like (cases 3 and 3'), depending on whether the restriction of the quadratic form $\mathbf{v} \mapsto \langle \mathbf{v}, \mathbf{v} \rangle$ to the plane is positive definite, indefinite or semi-definite, respectively. Using a suitable Lorentz transform we map it into one of the planes $r = 0$, $y = 0$ and $y - r = 0$, respectively. Within these planes, the unit vectors (characterized by $x^2 + y^2 - r^2 = 1$) form a circle, a hyperbola, and a pair of parallel lines (in the Euclidean sense), see Figure 6. Using another Lorentz transform one may map them to one of the canonical configurations listed in Table 2. \square

Table 2

Canonical positions of two space-like unit vectors $\mathbf{t}_0, \mathbf{t}_1$. The abbreviations sl., tl., and ll. stand for space-, time- and light-like, respectively.

| no. | s | d | canonical position | | |
|-----|-----|-----|------------------------------|-------------------------------|-----------------------------------|
| | | | \mathbf{t}_0 | \mathbf{t}_1 | $f \in$ |
| 1 | sl. | sl. | $(\cos f, \sin f, 0)^\top$ | $(\cos f, -\sin f, 0)^\top$ | $(-\frac{\pi}{2}, \frac{\pi}{2}]$ |
| 2 | sl. | tl. | $(\cosh f, 0, \sinh f)^\top$ | $(\cosh f, 0, -\sinh f)^\top$ | $(-\infty, \infty)$ |
| 2' | tl. | sl. | $(\cosh f, 0, \sinh f)^\top$ | $(-\cosh f, 0, \sinh f)^\top$ | $(-\infty, \infty)$ |
| 3 | sl. | ll. | $(1, 0, 0)^\top$ | $(1, f, f)^\top$ | $(0, \infty)$ |
| 3' | ll. | sl. | $(1, 0, 0)^\top$ | $(-1, f, f)^\top$ | $(0, \infty)$ |

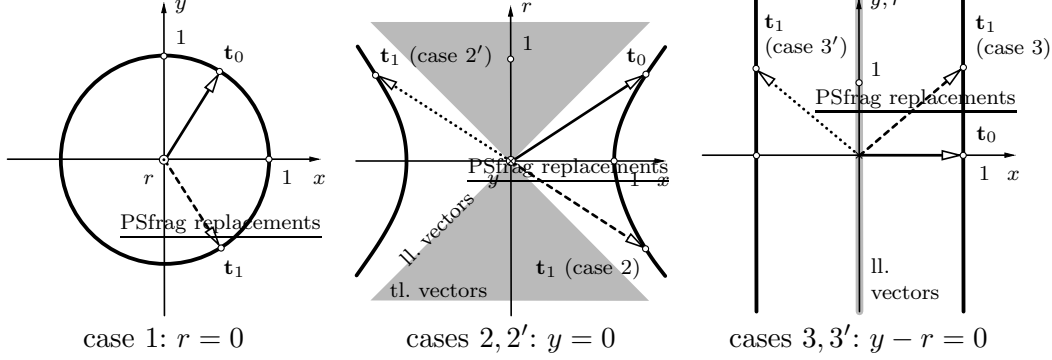


Fig. 6. The canonical positions of the plane spanned by the two vectors $\mathbf{t}_0, \mathbf{t}_1$, the curves formed by the unit vectors (bold) and the time-like resp. light-like vectors (interior and boundary of the grey regions in cases 2, 2' and 3, 3').

Remark 6 The remainder of this section studies the number of solutions for given G^1 input data. Later, in Section 5, we will analyze the behavior of piecewise G^1 Hermite interpolation of data taken from a space-like (possibly piecewise) analytic curve by MPH cubic splines. In this context, cases 2' and 3' from Proposition 5 cannot occur, provided that sufficiently close endpoints are chosen (see Section 5). Consequently, the solvability in these cases will not be analyzed now.

Moreover, since the interpolation procedure does not distinguish between the different possible orientations of the boundary tangents, cases 2 and 2' are equivalent, and the cases 3 and 3' are equivalent. Therefore, only the cases 1, 2 and 3 have to be addressed, which are distinguished by the causal character of $\mathbf{d} = \mathbf{t}_1 - \mathbf{t}_0$.

4.2 Solvability analysis

We study the solvability for the cases 1, 2 and 3 of the given input data, and for the (degenerate) case of linearly dependent boundary tangents. While cases 1 and 2 are regular (“generic”), case 3 and the degenerate case of linearly

dependent boundary occur for singular data.

4.2.1 Regular cases

Case 1: Space-like difference \mathbf{d} . We consider G^1 Hermite data, as specified in case 1 of Proposition 5. Recall that $\mathbf{p}_0 = (0, 0, 0)^\top$ and $\mathbf{p}_3 = (x, y, r)^\top$, see (24). The two equations (21) lead to

$$a = \frac{y + bs}{s} \quad \text{resp.} \quad a = \frac{x - bc}{c}, \quad (25)$$

depending on the choice of the sign, where $s = \sin f$ and $c = \cos f$. After using them to eliminate a from (22), we get the two quadratic equations

$$\begin{aligned} E_1 &= (8c^4 - 10c^2 + 2)b^2 + (-8sc^2y + 8s^2cx + 2sy)b - 2(sx - cy)^2 + 2r^2 = 0 \quad \text{and} \\ E_2 &= (8c^4 - 6c^2)b^2 + (-8sc^2y - 8c^3x + 6cx)b - 2(sx - cy)^2 + 2r^2 = 0. \end{aligned}$$

The roots of $E_1(b)$ (resp. $E_2(b)$), along with the a values obtained from the first (resp. second) equation (25), give the solutions of the first kind, resp. of the second kind. Clearly, these roots may be conjugate complex. Moreover, if $f \in \{0, \pm\frac{\pi}{6}, \pm\frac{\pi}{3}, \frac{\pi}{2}\}$, then one of the two quadratic equations degenerates into a linear one.

In the general case ($f \notin \{0, \pm\frac{\pi}{6}, \pm\frac{\pi}{3}, \frac{\pi}{2}\}$), the number of real solutions of the first or second kind depends on the signs of the discriminants D_1, D_2 with respect to the parameter b ,

$$\begin{aligned} D_1 &= 4s^2(4s^2x^2 + (1 - 4c^2)y^2 + (16c^2 - 4)r^2) \quad \text{resp.} \\ D_2 &= 4c^2((1 - 4s^2)x^2 + 4c^2y^2 + (16s^2 - 4)r^2). \end{aligned} \quad (26)$$

Consider a quadratic cone $C : \alpha x^2 + \beta y^2 + \gamma r^2 = 0$, where $\alpha\beta\gamma \neq 0$. A given point $\tilde{\mathbf{p}} = (\tilde{x}, \tilde{y}, \tilde{r})^\top$ is said to lie

$$\left. \begin{array}{l} \text{inside} \\ \text{on} \\ \text{outside} \end{array} \right\} \text{ the cone } C \text{ if } \alpha\tilde{x}^2 + \beta\tilde{y}^2 + \gamma\tilde{r}^2 \begin{cases} < 0 \\ = 0 \\ > 0 \end{cases}. \quad (27)$$

Fig. 7 visualizes the two families of quadratic cones D_1 resp. D_2 . Note that the x - resp. y -axis is always outside. The cones D_1 share the two common lines $(0, \pm 2t, t)^\top$, $t \in \mathbb{R}$ and two tangent planes $y^2 = 4r^2$ along them. Analogously, the cones D_2 share the two common lines $(\pm 2t, 0, t)^\top$, $t \in \mathbb{R}$ and the associated tangent planes $x^2 = 4r^2$.

Proposition 7 *For any given value of $f \in (-\frac{\pi}{2}, \frac{\pi}{2}) \setminus \{0, \pm\frac{\pi}{6}, \pm\frac{\pi}{3}\}$, the number of real solutions of the G^1 interpolation problem by MPH cubics with a space-like difference vector \mathbf{d} depends on the mutual position of the end point $\mathbf{p}_3 = (x, y, r)^\top \neq (0, 0, 0)^\top$ and the quadratic cones D_1, D_2 . If $\mathbf{p}_3 = (x, y, r)$ lies*

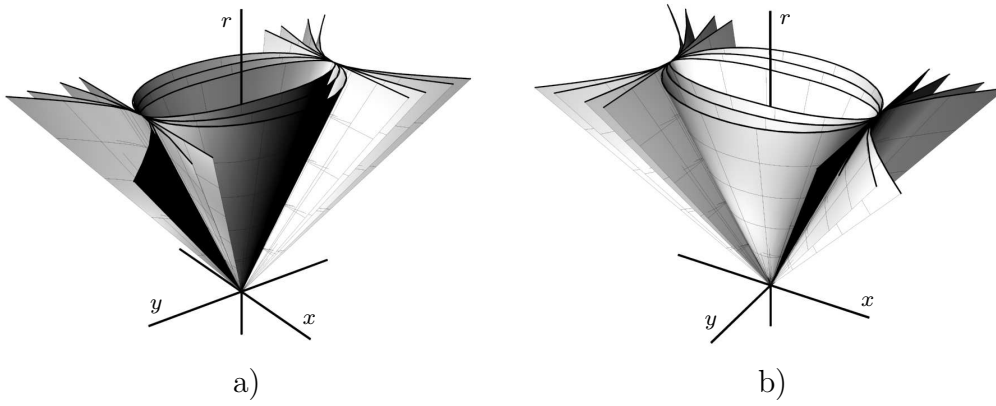


Fig. 7. Space-like difference vector \mathbf{d} : a) The family D_1 , and b) the family D_2 of quadratic cones for various values of the parameter f .

outside, on, or inside D_i , then the number of solutions of the i -kind equals two, one, or zero, respectively. In any case one obtains at least two real solutions.

Proof: The last part remains to be shown. By inspecting the two families of cones, one can verify that the interior parts of the cones do not intersect. Indeed, if $f \approx 0$, then the y -axis is inside D_1 and the r -axis is inside D_2 . If $f \rightarrow \pm\frac{\pi}{2}$, then the r -axis is inside D_1 and the x -axis is inside D_2 . \square

We conclude this section with a short discussion of singular cases.

- If $f = \frac{\pi}{3}$, then E_1 is linear in b and yields one solution when $x \neq 0$. If $x = 0$ then we obtain infinitely many or no solutions of the first kind, depending on whether $8r^2 - 2y^2 = 0$ or not. The second equation E_2 can be dealt with as in the regular case.
- If $f = \frac{\pi}{6}$, then E_2 is linear in b . The discussion of the number of solutions is analogous to the previous case.
- Coinciding endpoints, $\mathbf{p}_0 = \mathbf{p}_3 = (0, 0, 0)^\top$. The first equation (25) gives $a = b$, and $E_1 = 0$ implies $f = \pm\frac{\pi}{3}$. This is in perfect agreement with the fact that any planar PH curve of degree three is similar to a Tschirnhausen cubic (see Farouki & Sakkalis (1990)) as the angle between the tangents at the double point of the Tschirnhausen cubic equals $\frac{\pi}{3}$. The second case gives an equivalent result.
- The case of linearly dependent boundary tangents $f \in \{0, \frac{\pi}{2}\}$ will be analyzed in the last paragraph of Section 4.2.2.

Remark 8 Some solutions may have the wrong orientation ($a < 0$ or $b > 0$) or singular end points ($a = 0$ or $b = 0$). While this could be characterized by certain nonlinear inequalities for the components of \mathbf{p}_3 , we will present another approach in Section 5.

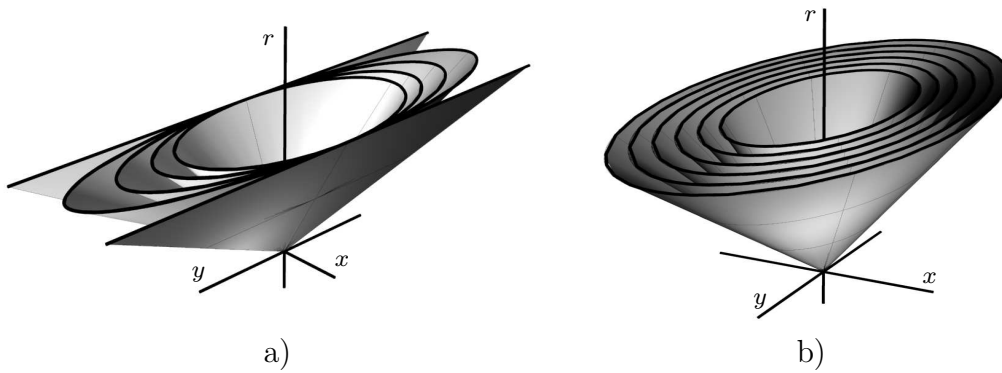


Fig. 8. Time-like difference \mathbf{d} : The family a) D_1 and b) D_2 of quadratic cones for various values of the parameter f .

Case 2: Time-like difference \mathbf{d} . The analysis in the case of a time-like difference vector \mathbf{d} is similar, but reveals a different behaviour. We consider G^1 Hermite data, as specified in case 2 of Proposition 5. The two equations (21) lead to

$$a = \frac{r + bS}{S} \quad \text{resp.} \quad a = \frac{x - bC}{C}, \quad (28)$$

depending on the choice of the sign, where $S = \sinh f$ and $C = \cosh f$. After using them to eliminate a from (22), we get the two quadratic equations

$$\begin{aligned} E_1 &= (8C^4 - 10C^2 + 2)b^2 + (8C^2r - 8SCx - 2r)Sb + 2(Sx - Cr)^2 - 2y^2 = 0 \quad \text{resp.} \\ E_2 &= (8C^4 - 6C^2)b^2 + (6Cx - 8C^3x + 8C^2Sr)b + 2(Sx - Cr)^2 - 2y^2 = 0 \end{aligned}$$

Their roots, along with the a values obtained from the first (resp. second) equation (28), give the solutions of the first kind, resp. of the second kind.

If $f = 0$, then the first equation degenerates into a linear equation. Otherwise, the number of real solutions of the first or second kind depends on the signs of the discriminants D_1 , D_2 with respect to the parameter b ,

$$\begin{aligned} D_1 &= 4S^2(4S^2x^2 + (16C^2 - 4)y^2 + (1 - 4C^2)r^2) \quad \text{resp.} \\ D_2 &= 4C^2((4S^2 + 1)x^2 + (16S^2 + 4)y^2 - 4C^2r^2). \end{aligned} \quad (29)$$

Similar to the previous case, we obtain two families of quadratic cones with apex at the origin, see Fig. 8. The r -axis is always inside both cones.

Proposition 9 *For any given value of $f \in \mathbb{R} \setminus \{0\}$, the number of real solutions of the G^1 interpolation problem by MPH cubics with a time-like difference vector \mathbf{d} depends on the mutual position of the end point $\mathbf{p}_3 = (x, y, r)^\top \neq (0, 0, 0)^\top$ and the quadratic cones D_1 , D_2 . If $\mathbf{p}_3 = (x, y, r)$ lies outside, on, or inside D_i , then the number of solutions of the i -kind equals two, one, or zero, respectively. As a sufficient condition, if $4y^2 - r^2 > 0$, then we get two solu-*

tions of the first kind, and if $\frac{1}{4}x^2 + y^2 - r^2 > 0$, then we obtain two solutions of the second kind.

Proof. The second part of the proposition can again be shown by analyzing the distribution of the cones. For $f \rightarrow \pm\infty$, both cones converge to the same limit cone $x^2 + 4y^2 - r^2 = 0$. For $f \rightarrow 0$, the cone D_1 converges to the two planes $4y^2 - r^2 = 0$, and D_2 converges to the limit cone $\frac{1}{4}x^2 + y^2 - r^2 = 0$. \square

The only singular case concerns coinciding endpoints, $\mathbf{p}_3 = (0, 0, 0)^\top$. This case does not have any solutions, except for $f = 0$. When \mathbf{d} is time-like, no planar MPH curve with a double point exists.

Remark 8 is again valid, but with possibly different signs for a and b , since cases 2 and 2' of Proposition 5 have been identified.

4.2.2 Singular cases

Case 3: Light-like difference \mathbf{d} . We consider G^1 Hermite data, as specified in case 3 of Proposition 5. The first of the two equations (21) implies $f = 0$ (which will be analyzed in the next section) or $y = r$. Consequently, for a general difference vector $\mathbf{p}_3 = (x, y, r)^\top$ with $y \neq r$ we do not obtain any solutions of the first kind. If $y = r$, then any choice of a, b gives an MPH cubic.

On the other hand, the second equation (21) leads to

$$a = x - b + \frac{1}{2}f(y - r) \quad (30)$$

After eliminating a from the second equation (22), we get

$$E_2 = 3bf(y - r) - 2(bx + y^2 - r^2 - b^2). \quad (31)$$

The discriminant of the quadratic equation E_2 has the form

$$D_2 = 4x^2 + (y - r)(16y + 16r + 9f^2y - 9f^2r - 12fx). \quad (32)$$

Similar to the regular cases, this equation defines a family of cones, see Fig. 9. For any given f and \mathbf{p}_3 , the number of solutions can be decided with the help of the corresponding cone in this family.

Degenerate case: Linearly dependent tangent vectors. We may assume that $\mathbf{t}_0 = \mathbf{t}_1 = (1, 0, 0)^\top$. Solutions of the first kind exist if and only if $y^2 = r^2$, and any choice of a, b then gives a solution. Solutions of the second kind exist if the discriminant $D_2 = 4x^2 + 16y^2 - 16r^2$ of E_2 is non-negative.

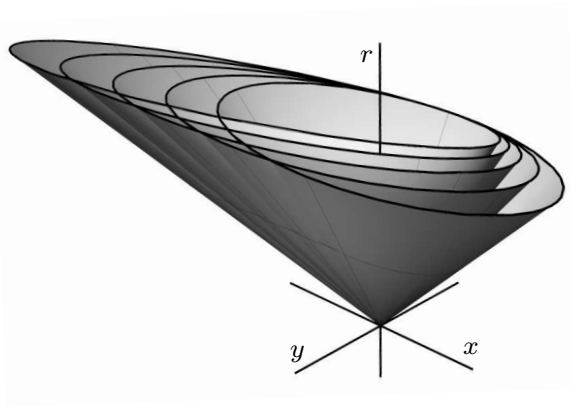


Fig. 9. Light-like difference \mathbf{d} : family $D_2 = 0$ of quadratic cones for various values of the parameter f .

5 Asymptotic analysis

As shown in the previous sections, the solvability of the G^1 Hermite interpolation problem depends heavily on the given data. In the remainder of the paper we take a different approach, as follows. We consider a curve segment $\mathbf{p} = \mathbf{p}(s)$ with $s \in [0, S_{max}]$ in Minkowski space, which is assumed to be space-like. The coordinate function are assumed to be analytic, and the parameter s is assumed to be the Minkowski arc length, i.e., $\langle \mathbf{p}', \mathbf{p}' \rangle = 1$.

For a given step-size h , we generate points and tangents at the points $s = ih$, $i = 0, 1, 2, \dots$ and apply the G^1 Hermite interpolation procedure by MPH cubics to the pairs of adjacent points and tangents. We analyze the existence and the behaviour of the solutions for decreasing step-size $h \rightarrow 0$.

5.1 Regular cases

Using the Frenet formulas (see Section 2.4) we generate a Taylor expansion of the given curve. The derivatives at $s = 0$ evaluate to

$$\begin{aligned} \mathbf{p}'(0) &= \mathbf{T}_0, \mathbf{p}''(0) = \mathbf{T}'(0) = \kappa_0 \mathbf{N}_0, \\ \mathbf{p}'''(0) &= \kappa_1 \mathbf{N}_0 + \kappa_0 \mathbf{N}'(0) = \kappa_1 \mathbf{N}_0 \mp (\kappa_0^2 \mathbf{T}_0 + \kappa_0 \tau_0 \mathbf{B}_0), \end{aligned} \quad (33)$$

etc., where $\mathbf{T}_0 = \mathbf{T}(0)$, $\mathbf{N}_0 = \mathbf{N}(0)$, $\mathbf{B}_0 = \mathbf{B}(0)$, $\kappa_0 = \kappa(0)$, $\kappa_1 = \kappa'(0)$, $\tau_0 = \tau(0)$, etc.. The choice of the sign in $\mathbf{p}'''(0)$ (and all further derivatives) depends on the causal character of the normal vector \mathbf{N}_0 . In the generic case, the normal vector \mathbf{N} is either space-like or time-like.

Note that the equations (33) are not valid at Minkowski inflections, where \mathbf{N}_0 is light-like. These cases have to be studied separately.

Using suitable initial conditions, we generate a Taylor expansion of the given curve,

$$\mathbf{p}(s) = \mathbf{p}(0) + s\mathbf{p}'(0) + \frac{s^2}{2}\mathbf{p}''(0) + \frac{s^3}{6}\mathbf{p}'''(0) + \dots \quad (34)$$

Without loss of generality, we choose $\mathbf{p}(0) = (0, 0, 0)^\top$, $\mathbf{T}_0 = (1, 0, 0)^\top$, and $\{\mathbf{N}_0, \mathbf{B}_0\} = \{(0, 1, 0)^\top, (0, 0, 1)^\top\}$, depending on the causal character of \mathbf{N}_0 .

We analyze the interpolants to the G^1 Hermite data sampled at s_0 and $s_1 = s_0 + h$. In the limit case $h \rightarrow 0$, the normal vector $\mathbf{N}(0)$ plays the role of the difference vector \mathbf{d} of the end tangent vectors.

Proposition 10 *Let $\mathbf{p}(s)$ be a space-like analytic curve with a space-like or time-like principal normal vector at $\mathbf{p}(s_0)$. Consequently, the Minkowski curvature satisfies $\kappa \neq 0$ at $\mathbf{p}(s_0)$. Then the G^1 Hermite interpolation of $\mathbf{p}(s)$ in $[s_0, s_0 + h]$ by MPH cubics has four solutions, provided that the step-size $h > 0$ is sufficiently small. Exactly one among them matches the shape of the given curve segment and possesses the approximation order four.*

Proof: Let $s_0 = 0$. If $\mathbf{N}(0)$ is space-like, then this remains valid for $s \in [0, h]$, provided that h is sufficiently small. The given curve has the Taylor expansion

$$\mathbf{p}(s) = \begin{pmatrix} s - \frac{1}{6}\kappa_0^2 s^3 - \frac{1}{8}\kappa_0\kappa_1 s^4 + \mathcal{O}(s^5) \\ \frac{1}{2}\kappa_0 s^2 + \frac{1}{6}\kappa_1 s^3 + \frac{1}{24}(\kappa_2 + \kappa_0(\tau_0^2 - \kappa_0^2))s^4 + \mathcal{O}(s^5) \\ \frac{1}{6}\kappa_0\tau_0 s^3 + \frac{1}{24}(2\kappa_1\tau_0 + \kappa_0\tau_0)s^4 + \mathcal{O}(s^5) \end{pmatrix}. \quad (35)$$

After sampling the Hermite boundary data at $s_0 = 0$ and $s_1 = h$, we generate Taylor expansions of the two quadratic equations $E_i(b) = 0$ and their discriminants,

$$\begin{aligned} D_1 &= \kappa_0^4 h^8 + 2\kappa_0^3 \kappa_1 h^9 + \mathcal{O}(h^{10}), \\ D_2 &= 4h^4 - \frac{16}{3}\kappa_0^2 h^6 - \frac{16}{3}\kappa_0\kappa_1 h^7 + \mathcal{O}(h^8). \end{aligned} \quad (36)$$

If h is sufficiently small, then the discriminants are positive and we obtain four real solutions.

The first solution of the first kind will be analyzed in more detail. The corresponding parameters a, b have the expansions

$$a_{1,1} = \frac{1}{3} + \frac{\kappa_1}{12\kappa_0}h + \mathcal{O}(h^2), \quad b_{1,1} = \frac{1}{3} - \frac{\kappa_1}{12\kappa_0}h + \mathcal{O}(h^2). \quad (37)$$

Hence, if h is sufficiently small, then the interpolant matches the orientations of the given tangent vectors. These parameters lead to the solution $\mathbf{q}(t) =$

$(\bar{x}(t), \bar{y}(t), \bar{r}(t))^\top$, where

$$\begin{aligned}\bar{x}(t) &= th + \frac{\kappa_1 t(1-t)}{4\kappa_0} h^2 + \mathcal{O}(h^3), \\ \bar{y}(t) &= \frac{1}{2}\kappa_0 t^2 h^2 + \frac{1}{12}\kappa_1 t^2(3-t)h^3 + \mathcal{O}(h^4), \\ \bar{r}(t) &= \frac{1}{6}\kappa_0 \tau_0 t^3 h^3 - \frac{1}{24}\tau_0(\kappa_0(1-2t) - \kappa_1(1+t)) + \mathcal{O}(h^5).\end{aligned}\tag{38}$$

This solution approximates the given analytic curve with the (geometric) approximation order 4, i.e.,

$$\mathbf{q}(t(\tau)) - \mathbf{p}(h\tau) = \mathcal{O}(h^4)\tag{39}$$

holds for all $\tau \in [0, 1]$ where $t(\tau)$ is a reparameterization $[0, 1] \rightarrow [0, 1]$,

$$t(\tau) = \tau + h\tau(\tau - 1)\frac{\kappa_1}{4\kappa_0} + h^2\tau(\tau - 1)\frac{L_1\tau + L_2}{96\kappa_0^2},\tag{40}$$

where

$$\begin{aligned}L_1 &= 10\kappa_1^2 + 8\kappa_0^2\tau_0^2 - 8\kappa_0^4, \\ L_2 &= 4\kappa_0^4 - 4\kappa_0^2\tau_0^2 - 17\kappa_1^2 + 12\kappa_0\kappa_2.\end{aligned}\tag{41}$$

The remaining three solutions can be analyzed in a similar way, see Kosinka (200x). It can be shown that the solutions of the second kind do not preserve the orientation of the boundary tangents, while the second solution of the first kind exhibits an ‘overshooting’ behaviour. The top row in Figure 12, page 23, visualizes the typical shape. These solutions do not match the shape of the given curve, and they do not possess the approximation order 4.

An analogous discussion can be given when the normal vector of \mathbf{p} at the origin is time-like. We obtain similar results, but by choosing the solution corresponding to the parameters $a_{1,2}$ and $b_{1,2}$ as the ‘best’ one. \square

5.2 Singular cases

Minkowski inflections correspond to points where the normal vector \mathbf{N} is light-like. This can be the case at an isolated point or within an entire interval.

Case 1: Isolated Minkowski inflection. We suppose that the normal vector of $\mathbf{p}(s)$ at the origin is light-like and the canonical Taylor expansion of $\mathbf{p}(s)$ at the origin has the form

$$\mathbf{p}(s) = s \begin{pmatrix} 1 \\ 0 \\ 0 \end{pmatrix} + \frac{s^2}{2} \begin{pmatrix} x_2 \\ y_2 \\ r_2 \end{pmatrix} + \frac{s^3}{6} \begin{pmatrix} x_3 \\ y_3 \\ r_3 \end{pmatrix} + \frac{s^4}{24} \begin{pmatrix} x_4 \\ y_4 \\ r_4 \end{pmatrix} + \begin{pmatrix} \mathcal{O}(s^5) \\ \mathcal{O}(s^5) \\ \mathcal{O}(s^5) \end{pmatrix}.\tag{42}$$

Table 3

Causal character of normal vector \mathbf{N} .

| j | y_j, r_j | $(-h_0, 0)$ | 0 | $(0, h_0)$ |
|------|-------------|-------------------------|-------------------------|-------------------------|
| odd | $y_j > r_j$ | time-like \mathbf{N} | light-like \mathbf{N} | space-like \mathbf{N} |
| odd | $y_j < r_j$ | space-like \mathbf{N} | light-like \mathbf{N} | time-like \mathbf{N} |
| even | $y_j > r_j$ | space-like \mathbf{N} | light-like \mathbf{N} | space-like \mathbf{N} |
| even | $y_j < r_j$ | time-like \mathbf{N} | light-like \mathbf{N} | time-like \mathbf{N} |

From equation $\langle \mathbf{p}'(s), \mathbf{p}'(s) \rangle = 1$, which holds for all s from some neighborhood of $s_0 = 0$, we obtain without loss of generality that $x_2 = 0$, $y_2 = \kappa$, $r_2 = \kappa$, $x_3 = 0$, $x_4 = \kappa(r_3 - y_3)$ etc. Therefore the expansion of $\mathbf{p}''(s)$ takes the form

$$\mathbf{p}''(s) = \kappa \mathbf{N} = \begin{pmatrix} 0 \\ \kappa \\ \kappa \end{pmatrix} + s \begin{pmatrix} 0 \\ y_3 \\ r_3 \end{pmatrix} + \frac{s^2}{2} \begin{pmatrix} 3\kappa(r_3 - y_3) \\ y_4 \\ r_4 \end{pmatrix} + \begin{pmatrix} \mathcal{O}(s^3) \\ \mathcal{O}(s^3) \\ \mathcal{O}(s^3) \end{pmatrix}. \quad (43)$$

Let j be the least index such that $y_j \neq r_j$, $j \geq 3$ (the case when j does not exist is considered in the paragraph addressing inflected segments). Then there exists an $h_0 > 0$ for which the normal vector \mathbf{N} of $\mathbf{p}(s)$ at the interval $(-h_0, 0)$, at the origin and at the interval $(0, h_0)$ has the causal character specified in Table 3.

This classification follows directly from the expansion of $\mathbf{p}''(s)$ and from the fact that $x_i = 0$ for every $2 \leq i \leq j$, $i \in \mathbb{N}$.

The discriminants D_1 , D_2 of the two quadratic equations for b have the expansions

$$\begin{aligned} D_1 &= k_j \kappa (r_j - y_j)^2 h^{2j+4} + \mathcal{O}(h^{2j+5}), \\ D_2 &= 4h^4 + \mathcal{O}(h^{4+j}), \end{aligned} \quad (44)$$

where k_j is a nonzero constant. Thus, all four solutions are real if $\kappa \neq 0$, provided that the stepsize h is sufficiently small. The case when $\kappa = 0$ yields an analogous result.

Similar to the previous section, we may identify the best solution. However, the geometric approximation order of this solution is only two. Consequently, *isolated Minkowski inflections reduce the approximation order*.

Case 2: Curve with inflected segments. This section analyzes a case which would not be present in the Euclidean world: a non-straight curve segment, where all points are inflection points.

More precisely, the normal vector is assumed to be light-like within an entire interval. This property characterizes curves which are contained in light-like planes. One boundary curve of the associated planar domain is a straight line

(the intersection of the light-like plane with the plane $r = 0$).

Proposition 11 *Let $\mathbf{p}(s)$ be a space-like analytic curve with a light-like normal vector for $s \in [s_0, s_0 + h]$, where $h > 0$. Then the G^1 Hermite interpolation of $\mathbf{p}(s)$ in $[s_0, s_0 + h]$ by MPH cubics has infinitely many solutions. For one of them the orientations of the tangent vectors are preserved and the approximation of $\mathbf{p}(s)$ is of order four.*

Proof: Following (8), we may suppose (without loss of generality) that $\mathbf{N}(0) = (0, \frac{\sqrt{2}}{2}, \frac{\sqrt{2}}{2})^\top$, $\mathbf{B}(0) = (0, \frac{\sqrt{2}}{2}, -\frac{\sqrt{2}}{2})^\top$. Then canonical Taylor expansion takes the form

$$\mathbf{p}(s) = \begin{pmatrix} s \\ \frac{\sqrt{2}}{4}s^2 + \frac{\sqrt{2}}{12}(\kappa_1 + \tau_0)s^3 + \mathcal{O}(s^4) \\ \frac{\sqrt{2}}{4}s^2 + \frac{\sqrt{2}}{12}(\kappa_1 + \tau_0)s^3 + \mathcal{O}(s^4) \end{pmatrix}. \quad (45)$$

In this case, the first equations (21), (22) are automatically satisfied. We obtain a two-parameter family of interpolants of the first kind, since the parameters a_1 and b_1 can be chosen arbitrarily. The coordinates of the interpolants $(\bar{x}(t), \bar{y}(t), \bar{r}(t))^\top$ have the expansions

$$\begin{aligned} \bar{x}(t) &= ((3a_1 + 3b_1 - 2)t^3 + (-6a_1 - 3b_1 + 3)t^2 + (3a_1)t)h, \\ \bar{y}(t) &= \bar{r}(t) = \frac{\sqrt{2}}{4}((6b_1 - 2)t^3 + (3 - 6b_1)t^2)h^2 + \mathcal{O}(h^3). \end{aligned} \quad (46)$$

By choosing $a_1 = b_1 = \frac{1}{3}$, the approximation order becomes four again and the interpolant matches the orientations of the boundary tangent vectors.

On the other hand, from the second set of equations (21), (22) we get $a_2 = 1 - b_2$, $E_2(b_2) = -2a_2b_2$ and therefore $a_{2,1} = b_{2,2} = 0$, $a_{2,2} = b_{2,1} = 1$. The interpolants of the second kind have a singular point at one of the segment boundaries. \square

5.3 Bounding the Hausdorff distance of planar domains

The Hausdorff distance between two circles with non-negative radii r_1, r_2 in the plane equals $\Delta r + \Delta c$, where $\Delta r = |r_1 - r_2|$ is the difference of the radii, and Δc is the distance between the centers. Consequently, the bound on the Euclidean distance between two curves in Minkowski space $\mathbf{p}(s)$, $\mathbf{q}(s)$ implies an upper bound on the Hausdorff distance between the associated planar domains,

$$\text{HD}(\Omega_{\mathbf{p}}, \Omega_{\mathbf{q}}) \leq \sqrt{2} \max_{s \in I} \|\mathbf{p}(s) - \mathbf{q}(s)\|_E \quad (47)$$

where $\|\cdot\|_E$ denotes the Euclidean norm. Therefore, the results on the approximation order of the MAT imply analogous results for the Hausdorff distance of the associated planar domains.

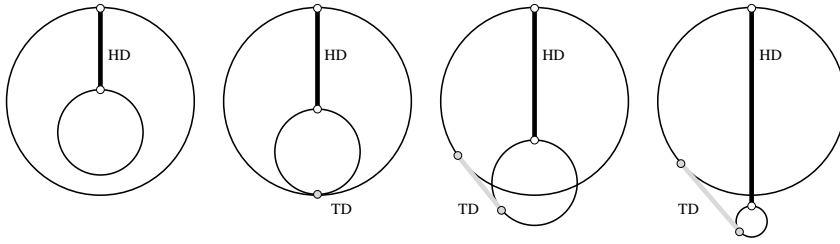


Fig. 10. Tangential distances (TD) vs. Hausdorff distances (HD) of two circles; the radii are assumed to be positive. In the first (resp. second) example, the tangential distance is imaginary (zero), since the difference vector between the points in Minkowski space describing the two circles is time-like (light-like).

Note that the Lorentz metric is not suitable for bounding the Hausdorff distance; it represents the so-called tangential distance between two circles, see Figure 10.

6 Examples

In this section we present numerical results obtained by applying the previously designed MPH approximation scheme. We consider the space-like cubic arc (the MAT of a planar domain Ω , cf. Fig. 11) $\mathbf{h}(t) = (t, t^2, \frac{t^3}{2})^\top$ with the parameter domain $t \in [0, 1]$.

Example 1. We apply the G^1 Hermite interpolation scheme to the curve segment obtained for $t \in [0, \frac{1}{2}]$, i.e., to the left half of the curve shown in Fig. 11.

The G^1 Hermite data are $\mathbf{h}(0) = (0, 0, 0)^\top$, $\mathbf{h}(\frac{1}{2}) = (\frac{1}{2}, \frac{1}{4}, \frac{1}{16})^\top$ and $\mathbf{h}'(0) = \mathbf{e}_1$, $\mathbf{h}'(\frac{1}{2}) = (1, 1, \frac{3}{8})^\top$. The algorithm described in Table 1 gives four solutions for parameters a and b :

$$\begin{aligned}
 \text{a) } & a_{1,1} = 0.128036, & b_{1,1} &= 0.184193, \\
 \text{b) } & a_{1,2} = 0.586249, & b_{1,2} &= 0.520228, \\
 \text{c) } & a_{2,1} = 0.811725, & b_{2,1} &= -0.158310, \\
 \text{d) } & a_{2,2} = -0.175181, & b_{2,2} &= 0.492110.
 \end{aligned} \tag{48}$$

The four interpolants in Minkowski space are shown in Fig. 12 (top row), along with the rational approximations to the original domain boundary $\partial\Omega$ (bottom). The first interpolant (black curve in the top left figure) is obviously the best one, and the given MAT cannot be visually distinguished from this curve. This fact was to be expected, since the normal vector of $\mathbf{h}(t)$ is space-like for every $t \in [0, \frac{1}{2}]$ (see Section 5.1).

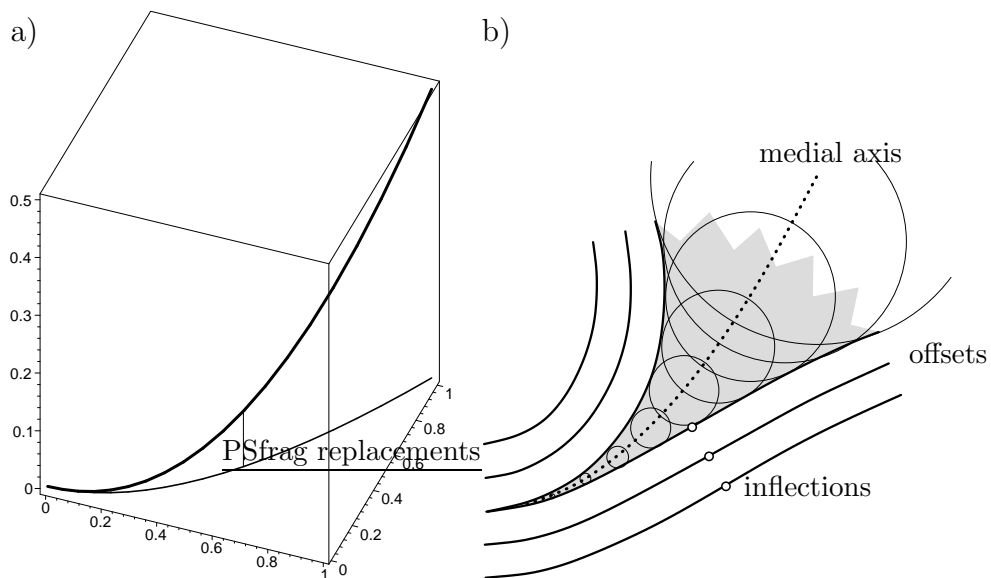


Fig. 11. (a) Curve in $\mathbb{R}^{2,1}$ with a Minkowski inflection point, (b) associated planar domain, its offsets and the inflections of the boundary.

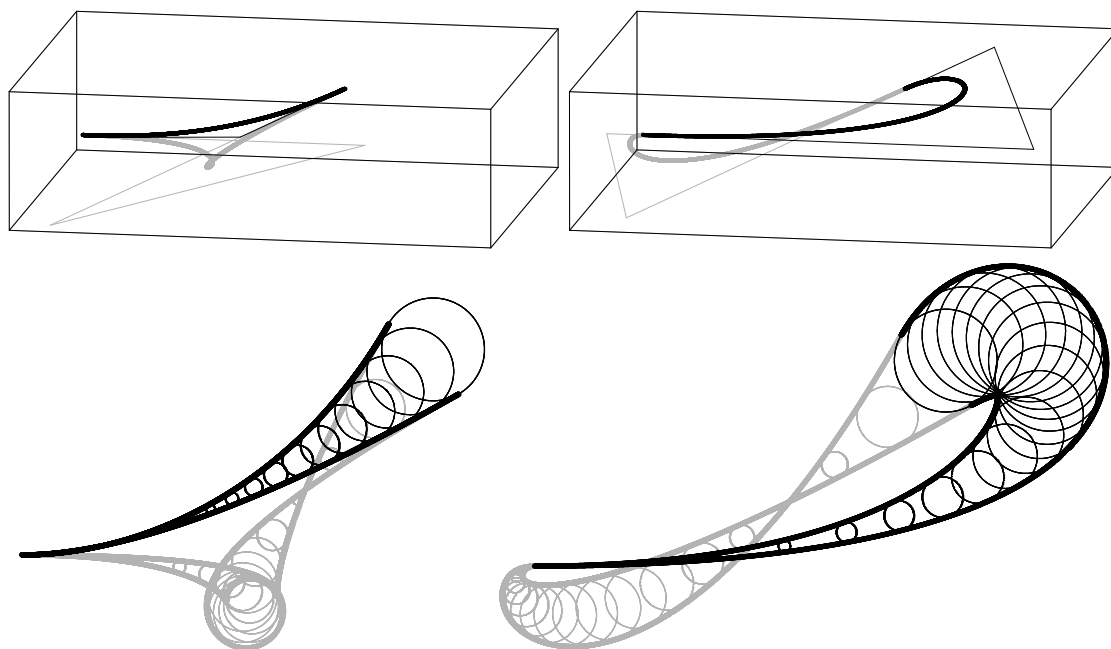


Fig. 12. Top: The four interpolants of Example 1 (black and grey, thick lines) and their control polygons (thin lines) in Minkowski space. Left: solutions of the first kind, right: solutions of the second kind. Bottom: The corresponding families of circles and their rational envelopes.

Table 4

Numerical results obtained by G^1 MPH interpolation and refinement via subdivision.

| i | $m_{i,1}$ | $m_{i,1}^\rho$ | $M_{i,1}$ | $M_{i,1}^\rho$ | $H_{i,1}$ | $H_{i,1}^\rho$ |
|-----|-----------------------|----------------|------------------------|----------------|------------------------|----------------|
| 0 | $2.253 \cdot 10^{-2}$ | — | $3.575 \cdot 10^{-3}$ | — | $3.286 \cdot 10^{-3}$ | — |
| 1 | $2.985 \cdot 10^{-3}$ | 7.548 | $2.389 \cdot 10^{-4}$ | 14.967 | $2.322 \cdot 10^{-4}$ | 14.151 |
| 2 | $3.861 \cdot 10^{-4}$ | 7.731 | $1.560 \cdot 10^{-5}$ | 15.307 | $1.549 \cdot 10^{-5}$ | 14.996 |
| 3 | $4.877 \cdot 10^{-5}$ | 7.918 | $9.887 \cdot 10^{-7}$ | 15.784 | $9.867 \cdot 10^{-7}$ | 15.694 |
| 4 | $6.112 \cdot 10^{-6}$ | 7.978 | $6.201 \cdot 10^{-8}$ | 15.943 | $6.198 \cdot 10^{-8}$ | 15.920 |
| 5 | $7.646 \cdot 10^{-7}$ | 7.995 | $3.879 \cdot 10^{-9}$ | 15.985 | $3.879 \cdot 10^{-9}$ | 15.980 |
| 6 | $9.559 \cdot 10^{-8}$ | 7.999 | $2.425 \cdot 10^{-10}$ | 15.996 | $2.425 \cdot 10^{-10}$ | 15.995 |

Example 2 Consider again the cubic arc of Example 1. We will interpolate $\mathbf{h}(t)$ using the G^1 MPH interpolation scheme and a binary subdivision. For the i -th level of subdivision ($i = 0, 1, 2, \dots$) and the n -th interval span $[\frac{n-1}{2^{i+1}}, \frac{n}{2^{i+1}}]$ we have the first order Hermite data $\mathbf{p}_{i,n-1} = \mathbf{h}(\frac{n-1}{2^{i+1}})$, $\mathbf{p}_{i,n} = \mathbf{h}(\frac{n}{2^{i+1}})$ and $\mathbf{t}_{i,n-1} = \mathbf{h}'(\frac{n-1}{2^{i+1}})$, $\mathbf{t}_{i,n} = \mathbf{h}'(\frac{n}{2^{i+1}})$, where $n = 1, \dots, 2^i$.

Following the results from Section 5.1 and Example 1 we consider the interpolant corresponding to $a_{1,1}$, $b_{1,1}$ only. We denote this interpolant $\mathbf{q}_{i,n}(s)$ and linearly reparameterize it to $s \in [\frac{n-1}{2^{i+1}}, \frac{n}{2^{i+1}}]$.

The numerical results are presented in Table 4. The values $m_{i,n}$, $M_{i,n}$ and $H_{i,n}$ are sampling-based estimates of various distances between the original curve $\mathbf{h}(t)$ and its interpolants. More precisely, we study the parametric distance

$$m_{i,n} = \max_t \{ \|\mathbf{q}_{i,n}(t) - \mathbf{h}(t)\|_E \}, \quad (49)$$

the parametric distance after the reparameterization (40)

$$M_{i,n} = \max_t \{ \|\mathbf{q}_{i,n}(\tau(t)) - \mathbf{h}(t)\|_E \} \quad (50)$$

and the Hausdorff distance

$$H_{i,n} = \max \{ \max_t \{ \min_s \{ \|\mathbf{h}(t) - \mathbf{q}_{i,n}(s)\|_E \} \}, \max_s \{ \min_t \{ \|\mathbf{h}(t) - \mathbf{q}_{i,n}(s)\|_E \} \} \},$$

where $s, t \in [\frac{n-1}{2^{i+1}}, \frac{n}{2^{i+1}}]$ and $\|\cdot\|_E$ denotes Euclidean norm. For each level of subdivision, only the distances obtained for the first segment ($n = 1$) are reported. Moreover, the ratios of two adjacent values for $i = 1, 2, \dots$ are shown, i.e. $m_{i,1}^\rho = \frac{m_{i,1}}{m_{i-1,1}}$, $M_{i,1}^\rho = \frac{M_{i,1}}{M_{i-1,1}}$ and $H_{i,1}^\rho = \frac{H_{i,1}}{H_{i-1,1}}$.

The numerically computed ratios confirm that the approximation order of the best solution is three resp. four before resp. after the reparameterization.

Example 3 The curve $\mathbf{h}(t) = (t, t^2, \frac{t^3}{2})^\top$ has Minkowski inflections for $t = \pm \frac{\sqrt{3}}{3}$ and $t = \pm \sqrt{2}$. Let us now take a closer look at the inflection $t = \frac{\sqrt{3}}{3}$.

Table 5

Numerical results obtained by G^1 MPH interpolation and refinement via subdivision at an inflection point.

| i | $m_{i,1}$ | $m_{i,1}^\rho$ | $M_{i,1}$ | $M_{i,1}^\rho$ | $H_{i,1}$ | $H_{i,1}^\rho$ |
|-----|-----------------------|----------------|-----------------------|----------------|-----------------------|----------------|
| 0 | $1.845 \cdot 10^{-1}$ | – | $1.438 \cdot 10^{-1}$ | – | $7.735 \cdot 10^{-2}$ | – |
| 1 | $8.404 \cdot 10^{-2}$ | 2.195 | $3.333 \cdot 10^{-2}$ | 4.098 | $1.981 \cdot 10^{-2}$ | 3.905 |
| 2 | $4.141 \cdot 10^{-2}$ | 2.029 | $7.948 \cdot 10^{-3}$ | 4.048 | $4.995 \cdot 10^{-3}$ | 3.966 |
| 3 | $2.049 \cdot 10^{-2}$ | 2.021 | $1.940 \cdot 10^{-3}$ | 4.024 | $1.254 \cdot 10^{-3}$ | 3.983 |
| 4 | $1.019 \cdot 10^{-2}$ | 2.012 | $4.791 \cdot 10^{-4}$ | 4.012 | $3.142 \cdot 10^{-4}$ | 3.991 |
| 5 | $5.078 \cdot 10^{-3}$ | 2.006 | $1.191 \cdot 10^{-4}$ | 4.006 | $7.864 \cdot 10^{-5}$ | 3.996 |
| 6 | $2.535 \cdot 10^{-3}$ | 2.003 | $2.968 \cdot 10^{-5}$ | 4.003 | $1.967 \cdot 10^{-5}$ | 3.998 |

Figure 11(a) depicts the curve $\mathbf{h}(t)$ for $t \in [0, 1]$ along with its projection to the xy plane. The parameter value $t = \frac{\sqrt{3}}{3}$ is marked by the thin line. Figure 11(b) shows the associated planar domain and the inflections of the boundaries, see Proposition 2.

The numerical data obtained from the subdivision scheme analogous to the one in Example 2 for the parameter interval $[\frac{\sqrt{3}}{3}, 1]$ are summarized in Table 5. Again, compare the values with the results of Section 5.2: the approximation order – after the reparameterization – is equal to two.

Remark 12 So far, curves with light-like tangents have been excluded. Still, such points may be present in applications, e.g., in the case of boundaries with vertices. If a point on the Minkowski space curve approaches a point with a light-like tangent, then the curvature goes to ∞ . The interpolation procedure can be adapted to this case, and the analysis of the number of solutions can be carried over. As observed in our numerical experiments, a ‘nice’ solution exists always, provided that the stepsize is sufficiently small. The approximation order of this solution is again equal to two, similar to the case of inflections. A thorough discussion to these cases will be given in the first author’s doctoral thesis (Kosinka, 200x).

7 Conclusion

As demonstrated in this paper, MPH curves can be used for approximating the medial axis transform of a planar domain. As an advantage, they admit a rational parameterization of the offset curves of the domain boundary. We have presented a general method for converting a space-like curve (MAT) into a G^1 spline via MPH cubics.

Based on the mutual position of the given first order Hermite data we derived the conditions for the existence and the number of interpolants. Using Taylor expansions we studied the approximation order, which is generally equal to

four, but it reduces to two at isolated Minkowski inflections.

In our future research we would like to analyze the C^1 interpolation via MPH quintics in Minkowski space $\mathbb{R}^{2,1}$ with the help of the Clifford algebra tools presented in Choi et al. (2002) and Cho et al. (2004).

Acknowledgment The first author was supported by the Austrian Science fund through project P17387-N12. The authors would like to thank the referees for their comments which have helped to improve the paper.

References

- Blaschke, W. (1929), Vorlesungen über Differentialgeometrie III, Springer, Berlin.
- Cho H. Ch., Choi, H. I., Kwon S.-H., Lee D. S., and Wee N.-S. (2004), Clifford algebra, Lorentzian geometry and rational parametrization of canal surfaces, *Comp. Aided Geom. Design*, 21, 327–339.
- Choi, H. I., Choi, S. W., and Moon, H. P. (1997), Mathematical theory of medial axis transform, *Pacific J. Math.*, 181(1), 57–88.
- Choi, H. I., Han, Ch. Y., Moon, H. P., Roh, K. H., and Wee, N. S. (1999), Medial axis transform and offset curves by Minkowski Pythagorean hodograph curves, *Comp.-Aided Design*, 31, 59–72.
- Choi, H. I., Lee, D. S., and Moon, H. P. (2002), Clifford algebra, spin representation and rational parameterization of curves and surfaces, *Adv. Comput. Math.*, 17, 5–48.
- Degen, W. L. F. (2004), Exploiting curvatures to compute the medial axis for domains with smooth boundary, *Computer Aided Geometric Design*, 21, 641–660.
- Ekmekci, N., and Ilarslan, K. (1998), Higher curvatures of a regular curve in Lorentzian space, *J. Inst. Math. & Comp. Sci.*, 11(2), 97–102.
- Farouki, R. T. (2002), Pythagorean-hodograph curves, *Handbook of Computer Aided Geometric Design* (J. Hoschek, G. Farin & M.-S. Kim, eds.), Elsevier, 405–427.
- Farouki, R. T., and Sakkalis T. (1990), Pythagorean hodographs, *IBM J. of Research and Development*, 34, 736–752.
- Kim, G.-I., and Ahn M.-H. (2003), C^1 Hermite interpolation using MPH quartic, 2003, *Computer Aided Geometric Design*, 20, 469–492.
- Kosinka, J. (200x), Algorithms for Minkowski Pythagorean Hodograph Curves, in preparation, Doctoral thesis, Faculty of Mathematics and Physics, Charles University, Prague.
- Moon, H. P. (1999), Minkowski Pythagorean hodographs, *Comp. Aided Geom. Design*, 16, 739–753.
- Pottmann, H., and Peternell, M. (1998), Applications of Laguerre geometry in CAGD, *Comp. Aided Geom. Design* 15, 165–186
- Walrave, J. (1995), Curves and surfaces in Minkowski space, Doctoral thesis, K. U. Leuven, Fac. of Science, Leuven.